

## Effect of ZrO<sub>2</sub> and L-Cys nanoparticles as dopants in sol-gel of mesoporous silica coating for corrosion protection of AZ61 magnesium alloy

Leonardo Hernández<sup>a</sup>, Lucien Veleva<sup>a,✉</sup>, Federico R. García-Galván<sup>b</sup>, Juan Carlos Galván<sup>b</sup>

<sup>a</sup>Center for Investigation and Advanced Study (CINVESTAV-IPN), Applied Physics Department, Carr. Ant. a Progreso km. 6, C.P. 97310, Merida, Yucatan, México

<sup>b</sup>Centro Nacional de Investigaciones Metalúrgicas (CENIM, CSIC), Avda. Gregorio del Amo, 8, 28040 Madrid, España

(✉)Corresponding author: [veleva@cinvestav.mx](mailto:veleva@cinvestav.mx)

Submitted: 9 July 2019; Accepted: 15 November 2019; Available On-line: 20 December 2019

**ABSTRACT:** Sol-gel coatings based on GPTMS-TMOS precursor, including as dopants L-Cysteine and ZrO<sub>2</sub> in different concentrations, were applied on the surface of AZ61 magnesium alloy. Their corrosion resistance was studied in 0.6M NaCl solution, by immersion up to 14 days. XRD spectra revealed Mg(OH)<sub>2</sub> as the main corrosion product on the coated surface, while on the untreated AZ61 in addition there were several compounds of Zn with chloride. The localized corrosion attack on the untreated AZ61 was expressed by cracks and caverns, while on the dip-coated surface the corrosion was mostly through pitting. Two non-destructive electrochemical methods were employed, contrasting the electrochemical behavior of coated AZ61 with that of uncoated alloy. The tendency in the changes of the corrosion potential at open circuit correlated positively with SEM-EDS and XRD analysis. The EIS diagrams were fitted to equivalent-circuit model and the obtained corrosion resistance R<sub>corr</sub> (R<sub>s</sub> + R<sub>ct</sub>) values strongly decreased over time. The ZrO<sub>2</sub> and L-Cysteine effect is influenced by the pH changes of the solution, Zeta potential surface charge, chemisorption and desorption processes, internal stress in the sol-gel precursor, as well as the change in its structure, after the encapsulation of both dopants.

**KEYWORDS:** AZ61; Corrosion; EIS; Magnesium alloy; Sol-gel coating; XRD

**Citation/Citar como:** Hernández, L.; Veleva, L.; García-Galván, F.R.; Galván, J.C. (2019). "Effect of ZrO<sub>2</sub> and L-Cys nanoparticles as dopants in sol-gel of mesoporous silica coating for corrosion protection of AZ61 magnesium alloy". *Rev. Metal.* 55(4): e155. <https://doi.org/10.3989/revmetalm.155>

**RESUMEN:** Efecto de las nanopartículas de ZrO<sub>2</sub> y L-Cys como agentes dopantes de recubrimientos sol-gel de sílice mesoporosa para la protección anticorrosiva de la aleación de magnesio AZ61. Sobre la superficie de la aleación de magnesio AZ61 se aplicaron recubrimientos de sol-gel basados en el precursor GPTMS-TMOS, incluyendo como agentes dopantes L-Cisteína y ZrO<sub>2</sub> en diferentes concentraciones. Su resistencia a la corrosión se estudió en solución de 0,6M NaCl, por inmersión hasta 14 días. Los patrones de DRX revelaron que el principal producto de corrosión en las superficies recubiertas es Mg(OH)<sub>2</sub>, mientras que en la de AZ61 no tratada adicionalmente se formaron varios compuestos de Zn con cloro. El ataque de la corrosión localizada en el AZ61 no tratada se manifiesta en forma de grietas y cavernas, mientras que en las superficies recubiertas la corrosión fue principalmente a través de picaduras. Dos métodos electroquímicos no destructivos fueron empleados en este estudio, que contrastan el comportamiento electroquímico del AZ61 recubierto con el de la aleación no recubierta. La tendencia en los cambios del potencial de corrosión en circuito abierto se correlacionó positivamente con el análisis SEM-EDS y DRX. Los diagramas EIS se ajustaron satisfactoriamente al modelo de circuito equivalente y los valores obtenidos de resistencia a la corrosión R<sub>corr</sub> (R<sub>s</sub> + R<sub>ct</sub>) disminuyen drásticamente con el tiempo de exposición. El efecto de ZrO<sub>2</sub> y L-cisteína están marcadamente influenciados por los cambios del pH de la solución, el potencial Zeta de la carga superficial, los procesos de quimisorción y desorción, el estrés interno en el precursor sol-gel, así como el cambio en su estructura, después de la encapsulación de ambos dopantes.

**PALABRAS CLAVE:** Aleación de magnesio; AZ61; Corrosión; DRX; EIS; Recubrimiento sol-gel

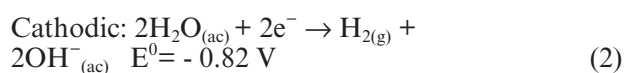
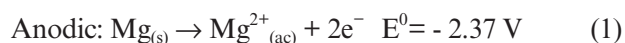
**ORCID ID:** Leonardo Hernández (<https://orcid.org/0000-0003-3326-9412>); Lucien Veleva (<https://orcid.org/0000-0003-1433-2885>); Federico R. García-Galván (<https://orcid.org/0000-0001-6349-8166>); Juan Carlos Galván (<https://orcid.org/0000-0002-8841-9716>)

**Copyright:** © 2019 CSIC. This is an open-access article distributed under the terms of the Creative Commons Attribution 4.0 International (CC BY 4.0) License.

## 1. INTRODUCTION

Magnesium (Mg) and its alloys have attracted the attention of the scientists as biodegradable medical materials for temporary implants in the human body (Zhang *et al.*, 2010). Because of their mechanical properties similar to those of natural bone, Mg-alloys have been widely studied and proposed in bone fixation (Wang and Shi, 2011). Another important feature is that Mg-based implants may degrade in contact with the physiological body fluids, releasing Mg ions through electrochemical corrosion process, thus eliminating the need for secondary extraction surgery (Park *et al.*, 2013). These implants may have greater benefits with the presence of drugs, as a low concentration of intentional drug can largely resolve local complications around the implant (Liu *et al.*, 2013). Therefore, this strategy has been applied in several devices, such as orthopedic implants. To meet this objective, the surface of the device is generally coated or modified to allow local administration of drugs.

The corrosion of Mg in aqueous solutions is faster in the presence of chloride ions and this leads to a rapid loss of mechanical strength of metal after its implantation. During the corrosion process, evolution of the hydrogen gas occurs (Eq. (4)), which may accumulate near the place where the implant was introduced, potentially damaging the surrounding tissues; likewise, bringing the local pH to alkaline values, because of the release of OH<sup>-</sup> ions (Liu *et al.*, 2013). The electrochemical corrosion develops according to the following reactions:



A physical barrier between the surface of the metal and the physiological body fluids could be created by coating the surface with a polymeric layer, which would also provide a mechanically strong bond with the bone (Zheludkevich *et al.*, 2006; Rueda *et al.*, 2016). In this case, the adhesion between the Mg and the polymer plays an important role in the useful life of the coating, which depends on its stability when loaded with drug nanoparticles (Park *et al.*, 2013). Several application techniques for thin film coating formation on metal surfaces have been used: for example, plasma deposition (Luo and Cui, 1998), chemical conversion (Hernández-Alvarado *et al.*, 2014) and the sol-gel method (Tan *et al.*, 2005; Supplit *et al.*, 2007; Zhong *et al.*, 2008; Minti *et al.*, 1991), among others.

The characteristics of sol-gel coatings make them suitable for reducing the corrosion degradation rate of the metal and their use is a recent but promising approach. Sol-gel coatings have demonstrated good chemical stability and control of oxidation (corrosion). Furthermore, the sol-gel technique is respectful towards the environment, without the need for specific pretreatment of the metal surface and the formed coatings provide a protective resistance for the metal, being nontoxic (Wang and Bierwagen, 2009). Other advantages are processing at low temperatures, simple and economical preparation. Sol-gel coatings have been applied on different materials, including those of Ti6Al4V implants (Gallardo *et al.*, 2003; Barranco *et al.*, 2014b).

Sol-gel hybrid coatings are more popular than the inorganic oxide layers formed on the metal surface in terms of protection against corrosion, for two main reasons (Wang and Bierwagen, 2009). First, hybrid coatings may form a thicker layer on a micrometer scale without cracks and use a much lower cure temperature (generally <100 °C) than 400–800 °C for oxide layers. Secondly, the hybrid sol-gel offers greater adaptation in terms of adhesion to anti-corrosion additives, such as inhibitors, paints, pigments, etc., so that the protection against general corrosion with sol-gel may be substantially improved (Wang and Bierwagen, 2009). The organic-inorganic hybrid compounds based on siloxane, prepared by the sol-gel technique, present unique properties that arise from the synergy between the properties of both components: they mix the properties of organic polymers (hardness, elasticity) with the properties of inorganic sol-gel (hardness, chemical resistance) (Novak, 1993; Judeinstein and Sanchez, 1996; Stein *et al.*, 2000; Gomez-Romero, 2001; Kahraman *et al.*, 2006).

Hybrid sol-gel coatings (Atik and Zarzycki, 1994; De Lima Neto *et al.*, 1994; Atik *et al.*, 1995; Caruso *et al.*, 2001; Gusmano *et al.*, 2007; Zhang *et al.*, 2007; Tamar and Mandler, 2008; Radhakrishnan *et al.*, 2009; Córdoba *et al.*, 2016) applied on metal surfaces have been manufactured using nanometric sized particles of TiO<sub>2</sub>, Al<sub>2</sub>O<sub>3</sub>, ZrO<sub>2</sub> and SiO<sub>2</sub>. Such coatings formed on aluminum are reported having a thickness of 7 μm, dense, smooth and inhibiting the corrosion of the metal substrate (Chen *et al.*, 1998). Sayilkan *et al.* (2003) reported the development of hybrid sol-gel coatings based on alkoxylan precursors, such as APS (Behzadnasab *et al.*, 2011; Mirabedini *et al.*, 2012), AEAPS, GPTMS (Montoya *et al.*, 2014) and MAPTMS (El-Hadad *et al.*, 2014), which showed good adhesion to the aluminum surface, as well as high chemical, mechanical and thermal stability. The properties of bioactivity and anticorrosive protection of organic-inorganic hybrid MAPTMS (g-methacryloxypropyltrimethoxysilane) and TMOS (tetramethylorthosilicate)

with a precursor phosphorus (triethylphosphite (TEP), have been also evaluated. The introduction of phosphorus has been carried to the molecular level in the hybrid organic-inorganic network (Barranco *et al.*, 2014b). TMOS is commonly used as an inorganic precursor in the manufacture of sol-gel coatings (Jiménez-Morales *et al.*, 2002; García-Heras *et al.*, 2004; Zheludkevich *et al.*, 2005; Barranco *et al.*, 2010; El-Hadad *et al.*, 2014). In another reported investigation (Storey and Rawlins, 2014), benzotriazole (BTA) and L-cysteine (L-Cys) were added as inhibitors in sol-gel (MAPTS-TMOS) to improve the efficiency of corrosion protection, as well as for the self-healing properties of the coating defects. After exposure to 0.006M NaCl, the coatings formed by MAPTMS/TMOS/BTA showed higher electrochemical impedance, because of the released BTA from the sol-gel surface and gradually blocked the defects of the coating. The formation of a stable adsorption layer on the surface of the Mg substrate is suggested, generating a good protection against corrosion in the active anodic areas of the metal (Guo *et al.*, 2009). Shchukin *et al.* (2006) also obtained similar results for BTA as inhibitor adsorbed on the surface of aluminum alloys, because of its release from the formed thin layer, hindering the corrosion processes. The coatings of MAPTMS/TMOS/L-Cys achieved impedances in the order of 10<sup>6</sup> Ω after 1 hour of exposure in chloride solution, which value is greater than 10<sup>5</sup> times that of unmodified coatings (MAPTMS/TMOS). After a longer time of exposure (14 hours), the impedance of the sol-gel films suffers a decrease. However, when they are doped with BTA and L-Cys, the change in the impedance is retained and it is about 10<sup>6</sup> Ω and 10<sup>5</sup> Ω, respectively, compared to that of coating without doping (10<sup>4</sup> Ω). The results of LEIS suggested that automatic recovery properties occur in the MAPTMS/TMOS/BTA films (Storey and Rawlins, 2014).

Other studies report the incorporation of hydroxyapatite particles (HAp) in the matrix of a hybrid sol-gel, resulting in more effective barrier properties and better protection against corrosion of Ti<sub>6</sub>Al<sub>4</sub>V alloy surface, covered by a suitable film thickness (Barranco *et al.*, 2014a). The silanes contain hydrolysable alkoxy-groups, which are converted to hydrophilic silanol groups (Si-OH). When these groups come into contact with metallic surfaces covered with hydroxyl-group (Me-OH), a condensation reaction takes place upon curing, forming metal-siloxane bonds (Me-O-Si) that cause the silane to adhere to the metal surface (Barranco *et al.*, 2014a). In the excess of Si-OH groups in the adsorbed layer, a siloxane network (Si-O-Si) is formed, which prevents the penetration of corrosive agents such as water, oxygen and chloride ions (Barranco *et al.*, 2014a). The corrosion resistance of the organic-inorganic hybrid coatings prepared with the sol-gel technique is based on the

properties of any existing physical barrier between the metal and the environment, so that a homogeneous coating free of defects is required (Barranco *et al.*, 2014a). Such coating should be uniform, a good adherent, pore-free and having a self-healing ability in the case of physical damage occurring in the coating surface (Gray and Luan, 2002). The use of coatings with Cr (VI) is prohibited, although they provide a good protection against corrosion, because of the release of these ions which are harmful to health and the environment (Gray and Luan, 2002).

The purpose of this work was the development and characterization of sol-gel hybrid coatings based on GPTMS+TMOS as precursors and doped with nanoparticles of ZrO<sub>2</sub> and L-Cys nanoparticles, considered as inhibitor for protection of the commercial magnesium alloy AZ61 surface against the corrosion. For the choice of the appropriate concentration for the composition of GPTMS + TMOS + L-Cys and GPTMS + TMOS + ZrO<sub>2</sub>, the yield of GPTMS + TMOS coatings with the addition of ZrO<sub>2</sub> and L-Cys in different concentrations was evaluated after each coating exposure for 14 days in 0.6M NaCl solution. Later, the selected hybrid sol-gel coating was loaded with both nanoparticles to obtain GPTMS + TMOS + L-Cys + ZrO<sub>2</sub> coating. The research was carried out with different electrochemical and surface analysis methods, such as measurement of the open circuit potential value (OCP), Electrochemical Impedance Spectroscopy (EIS), Scanning Electron Microscopy (SEM) and X ray Diffraction (XRD).

## 2. MATERIALS AND METHODS

### 2.1. Samples and solution preparation

The commercial rolled AZ61B, supplied by Magnesium Elektron (UK), was employed as test material and its provided certified composition (wt.%) is: 6.2 Al; 0.74 Zn; 0.23 Mn; 0.04 Si; 0.004 Fe; 0.0013 Ca and the balance Mg. The square samples (2 x 3 x 0.3 cm) were cut and abraded with 350, 500, 1200 and 2000 grit SiC paper and mirror polished with 3-μm and 1-μm diamond paste. The 0.6 M NaCl solution was prepared from analytical grade reagent (Sigma-Aldrich, St. Louis, MO, USA) and ultrapure deionised water (18.2 MΩ·cm).

### 2.2. Sol-gel hybrid coating

The sol-gel precursor was composed by GPTMS ((3-glycidioxypropyl) trimethoxysilane) and the inorganic TMOS (tetramethyl orthosilicate), in a proportion of 4:1 by weight, both added to ethanol-water solution and acetic acid (HAc) as catalyst. The pH of the obtained sol-gel was maintained at a constant value of 4.0.

Nanoparticles of L-Cys (L-cysteine) were incorporated into the sol-gel precursor in three molar concentrations: 0.3, 0.6 and 0.9%, each amount of these added to 20 ml of the sol-gel precursor and mixed for 24 h with a magnetic agitator. The ZrO<sub>2</sub> obtained from zirconium (IV) tert-butoxide (ZTB) was also evaluated for three molar concentrations: 0.3, 0.6 and 0.9%, each amount of this was also added to 20 ml of the sol-gel precursor and mixed for 24 h with a magnetic agitator. In the alcohol-water solution of the sol-gel precursor, ZTB undergoes very rapid hydrolysis, so that flocs and zirconia precipitates tend to form. The addition of a small amount of acetyl acetone (HacAc) and deionised water allows the Zr<sup>4+</sup> ions to remain coordinated (Barranco *et al.*, 2010).

The experiments in this study were carried out with the mixture of the sol-gel precursor and inhibitors of ZrO<sub>2</sub> and L-Cys, chosen in those concentrations that showed better protection resistances for AZ61, according to the Nyquist and Bode (EIS) diagrams.

The hybrid sol-gels were deposited on the metal samples, using an elevator, in such a way that the speed of immersion and ascent of the sample could be controlled. The speed was 3 mm·s<sup>-1</sup>, without keeping the samples submerged between the two events. Once out of the solution, the samples were suspended vertically inside a convection oven (Heraeus) for 3 hours, curing at 80 °C. The appearance of the coating was examined with the naked eye with respect to color, transparency, uniformity, homogeneity or any present defect.

### 2.3. Electrochemical tests (EIS)

The experimental setup consisted of a three-electrode cell (inside a Faraday cage) as follows: a saturated Ag/AgCl/KCl reference electrode, a platinum spiral as a counter electrode and AZ61 samples as working electrode. The cell was connected to Metrohm / EcoChemie Autolab PGSTAT302N potentiostat/galvanostat, equipped with a FRA32M frequency response analyzer module and a PARSTAT 4000 potentiostat. The AZ61 samples (working electrodes) were exposed to 100 ml of 0.6M NaCl solution at temperature of 21 ± 1 °C, for different periods of time (0 h, 1 h, 3, 5, 7 and 14 days) and before the EIS measurements the open circuit potential (E<sub>oc</sub>) was recorded. The EIS measurements were conducted at OCP conditions, applying 10 mV sinusoidal signal amplitude with frequencies ranging from 10<sup>-5</sup> to 10<sup>-2</sup>

Hz, taking 10 points per decade. The surface exposed to the electrolyte was 1.0 cm<sup>2</sup> delimited by a circular ring of rubber. All tests were repeated at least 3 times to verify the repeatability of the results. The Elchem Analyst™ Gamry's dedicated data-analysis program was used to build an equivalent-circuit model and then to fit that model to experimental data.

### 2.4. Microstructure characterization

The SEM-EDX Phillips and XL-30 ESEM JEOL JSM-7600F scanning microscopes were used to characterize the morphological and elemental changes occurring on the surface of AZ61 coated with sol-gel samples, after their immersion in 0.6M NaCl. Their surfaces were treated previously with a solution composed of CrO<sub>3</sub>, AgNO<sub>3</sub>, Ba(NO<sub>3</sub>)<sub>2</sub> and water, according to the ISO 8407 (1991) to remove only the corrosion layers, rinsed with distilled water and ethanol, then dried in warm air flow. The crystalline phases of the formed corrosion products were identified by X-ray diffraction technique (D8 Advance diffractometer Bruker) with Bragg geometry of 0.5-second step time (0.02 step size rotation), 3° angle, Cuka radiation and 34 kV/25 mA.

## 3. RESULTS AND DISCUSSION

### 3.1. Open circuit potential (E<sub>oc</sub>)

Table 1 presents the steady-state values of the open circuit potential, measured after exposure of untreated AZ61 and sol-gel coated samples, varying the concentration of the L-Cys and ZrO<sub>2</sub>, exposed for 14 days to 0.6M NaCl. This information was used to compare the corrosion behavior of the studied systems, with an addition of L-Cys and ZrO<sub>2</sub>, introduced in the sol-gel coatings in different concentrations. It may be noted that at the end of this experiment the AZ61 sol-gel coated (GPTMS+TMOS precursors) sample showed an E<sub>oc</sub> value of 20 mV less negative than that of the AZ61 untreated surface. The addition of 0.3% L-Cys or 0.6% ZrO<sub>2</sub> had a more significant effect on E<sub>oc</sub>, shifting the values to less negative.

### 3.2. Electrochemical impedance spectroscopy (EIS)

In the search for a sol-gel hybrid coating that delays the corrosion process of the AZ61 Mg alloy, the Nyquist and Bode diagrams of the coatings

TABLE 1. Values of E<sub>oc</sub> of sol-gel coatings applied on AZ61 surface after exposure to 0.6M NaCl at 21 °C for 14 days

E <sub>oc</sub> (V)	AZ61	Sol-Gel (precursors)	+0.3% L-Cys	+0.6% L-Cys	+0.9% L-Cys	+0.3% ZrO <sub>2</sub>	+0.6% ZrO <sub>2</sub>	+0.9% ZrO <sub>2</sub>
14 days	-1.58 ± 0.002	-1.56 ± 0.002	1.52 ± 0.002	1.55 ± 0.002	-1.55 ± 0.002	-1.56 ± 0.002	-1.54 ± 0.002	-1.55 ± 0.002

(Table 1) were compared, after exposure in 0.6M NaCl (21°C) to different periods, from zero hours to 14 days (Fig. 1). Bode diagrams (Fig. 2) were used to obtain the values of the corrosion resistance  $R_{\text{corr}}$  ( $R_s + R_{\text{ct}}$ , solution resistance and charge transfer resistance, respectively) at zero time and after 14 days of exposure to 0.6M NaCl (Table 2). It can be noted that L-Cys does not present inductive arc at low frequencies; however, for ZrO<sub>2</sub> it is well pronounced at 0.3% and 0.9%, as well for sol-gel precursor. The absence of inductive arc may be a consequence of the difference in the porosity of the compared sol-gel coatings. The changes of  $R_{\text{corr}}$  values with the time of exposure (Table 2) could indicate that in the presence of the aggressive chloride ions the surface of AZ61, as well the layers of sol-gel coatings, have undergone transformation. The Nyquist diagrams and the values of  $R_{\text{corr}}$  (Table 2) of the studied systems suggested that the addition of 0.6% ZrO<sub>2</sub> and 0.3% L-Cys could be optional additives, which could provide better

corrosion resistance of sol-gel hybrid based on GPTMS+TMOS precursors, applied as coating on AZ61 surface.

The electrochemical behavior of the newly formed sol-gel hybrid coating was monitored by Nyquist and Bode EIS diagrams, during its exposure to 0.6M NaCl for 14 days. Figure 3 presents the initial and final (at 14 days) diagrams. The corrosion process was mainly controlled by the charge transfer resistance ( $R_{\text{ct}}$ ) and at the end of this experiment one order of decrease in  $R_{\text{ct}}$  value was observed, as an indication for surface changes.

Figure 4 presents the equivalent-circuit model built, fitted to the experimental EIS data (Fig. 3) and the characteristic EIS parameters are resumed in Table 3. The constant phase element CPE1 (Fig.4), as a part of the equivalent circuit, describes the behavior of the double layer as an imperfect capacitor, because of the heterogeneity of AZ61-coating-electrolyte interface and its value is a function of the sol-gel coating thickness: the greater the thickness,

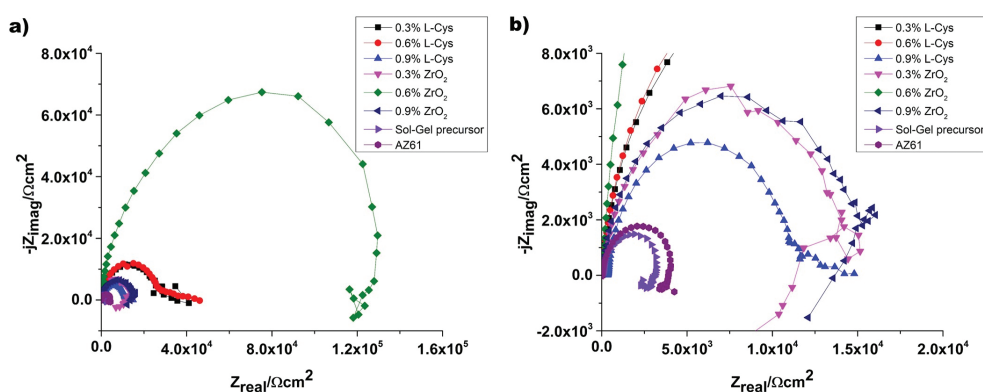


FIGURE 1. (a) Nyquist diagrams of AZ61 surfaces, untreated and dip-coated with different sol-gel hybrid systems, after zero time of exposure to 0.6M NaCl (21 °C); (b) zoom of Nyquist arcs.

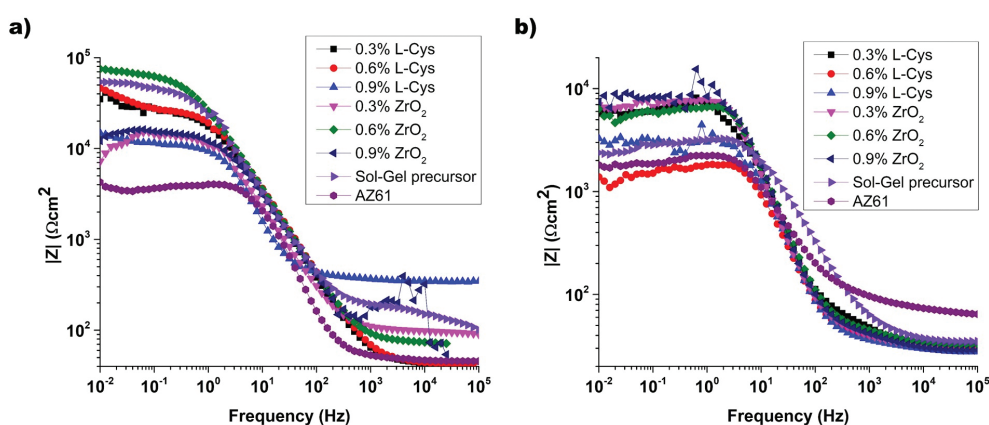


FIGURE 2. Bode diagrams of AZ61 surfaces, untreated and dip-coated with different sol-gels hybrid systems, after exposure to 0.6M NaCl: (a) at zero time and (b) after 14 days.

TABLE 2. Values of  $R_{\text{corr}}$  ( $R_s + R_{\text{ct}}$ ) of AZ61 surfaces, untreated and dip-coated with different sol-gels hybrid systems, after 14 days of exposure to 0.6M NaCl (21 °C)

$R_{\text{corr}}$ $k\Omega \cdot \text{cm}^{-2}$	AZ61 untreated	Sol-Gel precursor	+0.3% L-Cys	+0.6% L-Cys	+0.9% L-Cys	+0.3% $\text{ZrO}_2$	+0.6% $\text{ZrO}_2$	+0.9% $\text{ZrO}_2$
0 h	4.26	54.10	33.81	45.29	14.77	15.00	75.10	11.28
14 days	1.61	2.38	5.73	1.39	3.28	6.05	6.37	7.45

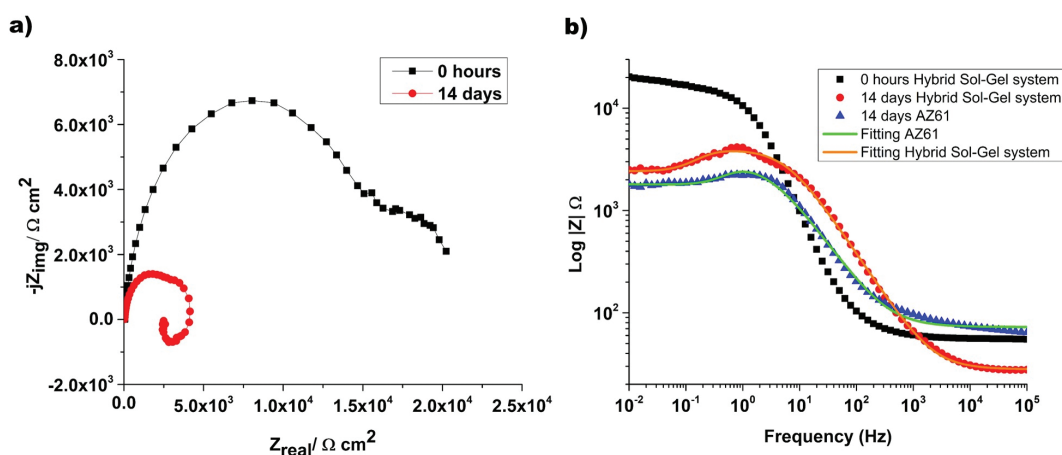
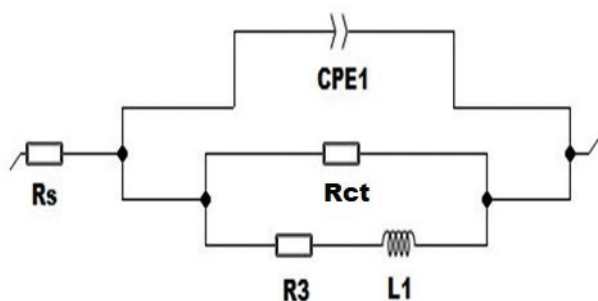
FIGURE 3. Nyquist (a) and Bode (b) diagrams of AZ61 surface and surface coated with hybrid sol-gel system (GPTMS-TMOS + 0.3% L-Cys + 0.6%  $\text{ZrO}_2$ ), during its exposure to 0.6M NaCl (21 °C) for 14 days.

FIGURE 4. Equivalent-circuit model based on Bode EIS diagrams for untreated AZ61 surface and dip-coated with hybrid sol-gel system, after 14 days of exposure to 0.6M NaCl (21°C).

the lower the value. Meanwhile, the components  $R_3$  and  $L1$  (resistance and inductor, respectively) could be associated with phenomena of adsorption-desorption of species, which alter the electrode potential and AZ61 corrosion rate (Aperador Chaparro *et al.*, 2012). The values of  $n$  component (Fig. 4 and Table 3) are a function of the surface imperfection and roughness: value of 1.0 corresponds to perfectly smooth surface. The value of  $\text{Chi}$  in the order of  $10^{-3}$  is acceptable (Table 3), because the corrosion process of such system is very complex.

### 3.3. SEM-EDS and XED analysis

SEM-EDS and XRD techniques provided an additional information for the changes that have occurred on the untreated AZ61 surface and that of dip-coated with the hybrid system (GPTMS-TMOS+0.3%L-Cys+0.6%  $\text{ZrO}_2$ ), after their exposure for 14 days to 0.6M NaCl. Figure 5 compares the morphology of AZ61 surfaces, untreated and dip-coated, after removal of the corrosion layer and coating. The corrosion attack (Fig. 5a) on the untreated AZ61 surface is well localized in cracks, forming caverns, where the  $\text{Cl}^-$  ions have penetrated the alloy surface, promoting the deterioration of the Mg-matrix. On the dip-coated surface, the corrosion attack mostly occurs through pitting with a different diameter size.

EDS elemental analysis of several zones on the AZ61 untreated surface (Fig.5a), whose exhibit distinctive morphologies after the removal of the corrosion layer, revealed that Mg presents the largest content (in the zones A and B), contributed by the matrix of the alloy. The detected Al (6.43 wt. %) and Zn (0.77 wt. %) are as part of the AZ61 magnesium alloy composition. The elemental content of the zone C may correspond to sites of  $\text{Al}_8\text{Mn}_5$ , as intermetallic inclusions nucleated in the  $\alpha$ -Mg grains (Pan *et al.*, 2012), in the presence of NaCl. Manganese is one of the common elements added

TABLE 3. Values of EIS equivalent-circuit (Fig.4) components presenting untreated AZ61 surface and dip-coated with hybrid sol-gel system (GPTMS-TMOS precursor + 0.3% L-Cys + 0.6% ZrO<sub>2</sub>), after 14 days of exposure to 0.6M NaCl (21 °C)

Sample	R <sub>s</sub> (Ω)	R <sub>ct</sub> (kΩ)	R <sub>3</sub> (kΩ)	L1 (H)x10 <sup>3</sup>	CPE1 (S*s <sup>n</sup> )x10 <sup>-5</sup>	n	Chi x10 <sup>-3</sup>
AZ61 Untreated	72.24	2.78	4.59	1.84	2.98	0.81	7.87
Sol-Gel hybrid	27.9	3.98	6.03	8.37	1.08	0.85	3.69

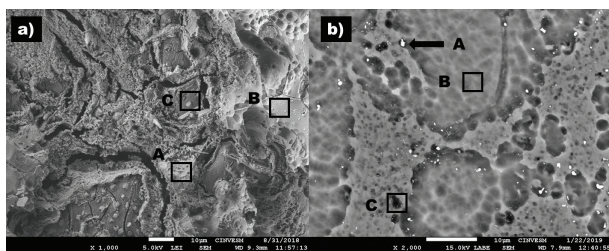


FIGURE 5. a) Untreated AZ61 surface and b) dip-coated with hybrid sol-gel system, after 14 days of exposure to 0.6M NaCl (21 °C); the corrosion layer and coating have been removed.

to most commercial magnesium alloys, essential for enhancing the corrosion resistance and these intermetallic particles are usually present in most of commercial Mg–Al based alloys (Han and Liu, 2016). The simulation of the micro-galvanic cathodic behavior of Al-Mn intermetallic particles has confirmed their cathodic behavior and the deposition of the corrosion products occurs in the vicinity with the active anodic  $\alpha$ -Mg grains, in the presence of chloride ions (Asmussen *et al.*, 2016). This fact explains the persistence of these particles on the alloy surface after the removal of the corrosion layer. The presence of the oxygen in each morphological zone may indicate the surface of the Mg-matrix with its native oxides, such as MgAl<sub>2</sub>O<sub>4</sub> and MgO.

On the dip-coated AZ61 surface with the hybrid sol-gel system (GPTMS-TMOS precursor + 0.3% L-Cys + 0.6% ZrO<sub>2</sub>), “white” particles and two distinctive morphologies are observed, after the removal of corrosion layer and coating (Fig. 5b). The “white” particles present high content of Al (13.33 wt.%) and Mn (6.25 wt.%), which may correspond to sites of Al<sub>8</sub>Mn<sub>5</sub>, as intermetallic inclusions. The C content (19.72 wt.%) could be considered as sol-gel residues strongly encapsulated on the Mg surface. The elemental content of the zones A and B corresponds to that of AZ61 alloy. The “black area” (zone C) contains C, N, Si and S, and it was associated with the hybrid sol-gel residues.

According to reports, it is considered that the corrosion products formed on Mg-alloys surfaces consist of three layers, varying in the content of O and Mg, which concentrations increase in the internal sublayer, as a part of corroded Mg-Al-Zn alloy surface (Afrin *et al.*, 2008; Hamu *et al.*, 2009; Aperador Chaparro *et al.*, 2012).

Figure 6 compares the XRD spectra of the corrosion products formed on untreated AZ61 surface with those on dip-coated, after exposure for 14 days in 0.6M NaCl. The results indicate that the main corrosion product on the hybrid surface is Mg(OH)<sub>2</sub> brucite, while on the untreated AZ61 surface in addition to brucite there are several compounds of Zn with chloride, in the presence of NaCl.

### 3.4. ZrO<sub>2</sub> and L-Cysteine as dopants in GPTMS-TMOS precursor

The values of R<sub>corr</sub> (R<sub>s</sub> + R<sub>ct</sub>) of AZ61 surfaces, dip-coated with different sol-gel hybrid systems (Table 3), exposed to 0.6M NaCl (21°C), lead to several conclusions. For example, at the initial time R<sub>corr</sub> value of the sol-gel precursor + 0.6% ZrO<sub>2</sub> (75.10 kΩ cm<sup>-2</sup>) was twice higher than that of sol-gel precursor + 0.3% L-Cys (33.81 kΩ cm<sup>-2</sup>), when the effect is compared of both additives used for the selected hybrid sol-gel coating (GPTMS-TMOS + 0.3% L-cys + 0.6% ZrO<sub>2</sub>) in this study. However, at the end of the experiment (14 days) their R<sub>corr</sub> values were relatively similar (Table 3).

The Zeta potentials of ZrO<sub>2</sub> have been measured in 1mM NaCl (Liu *et al.*, 2002) and the reported isoelectric point (pH<sub>iep</sub>-value) was 4.9 for ZrO<sub>2</sub>. At low pH = 2, ZrO<sub>2</sub> forms stable colloidal particles with a positive zeta potential (+15 mV) and in the vicinity of the pH<sub>iep</sub>, the particles turn their Zeta potential to negative value, reaching -30 mV up to pH=10. Then, taking into account the initial pH = 6.8 of the 0.6 M NaCl, used as a solution for testing, ZrO<sub>2</sub> should have a positive Zeta potential on the surface, and indeed even later when pH increases (Eq. 2). As a consequence, the surface should attract the negative charge of the chloride ions.

It has also reported that ZrO<sub>2</sub> presents high adsorption capacity (Liu *et al.*, 2008) with respect to PO<sub>4</sub>(3-) anions in water solution (with acid pH), and the adsorption data fitted well to the Langmuir model. However, in the alkaline solution of 0.5 M NaOH, phosphate desorbability of approximately 60% was observed. The authors conclude that the adsorption tended to decrease with the increase in pH, when the desorption process starts to dominate.

On the other hand, it was reported that the molecule of L-Cysteine is stable in pH between 3 and 7, having a neutral charge (zero) (Zhang *et al.*,

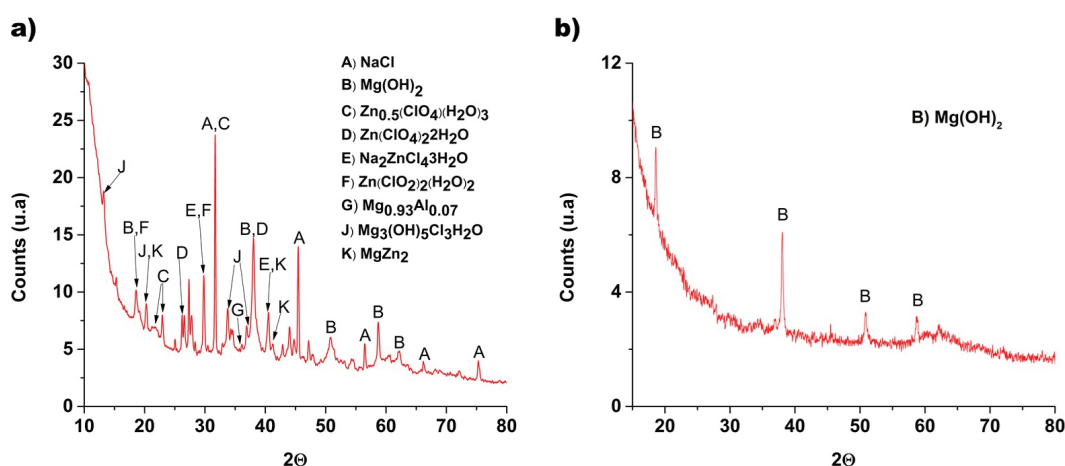


FIGURE 6. XRD spectra of corrosion products formed on AZ61 surface: (a) untreated and b) dip-coated (GPTMS-TMOS precursor + 0.3% L-Cys + 0.6% ZrO<sub>2</sub>), after exposure for 14 days to 0.6M NaCl.

2015). As a consequence, it might be suggested that in 0.6M NaCl electrolyte, L-Cys cannot repel the entry of chloride ions in the sol-gel coating or attract them to the surface. At pH = 0 - 2.9, it is considered that the L-Cyst cationic form appears, whose stability domain is very narrow and at pH » 9 it is transformed into its mono-negative anionic form, followed by the double-negative anionic form when the pH > 12; the latter occurs because of the deprotonation of the thiol group. It can be expected that with the increase in pH to more alkaline values (Eq. 2), both anionic forms of L-Cys could be formed, but also released to the solution of NaCl. For this reason, we suggest that the incorporation of L-Cys to the sol-gel precursor does not provide a contribution to the increase of the hybrid sol-gel coating corrosion resistance.

It was further reported (Sunwoo *et al.*, 2000; Mocanu *et al.*, 2009; Ma *et al.*, 2016) that L-Cys could serve as a container for metal ions released during the corrosion of AZ61 (Mg, Si, Al, Zn, Mn, Table 5), which can lead to internal stresses in the precursor layer and loss of adhesion of ZrO<sub>2</sub> particles. Both facts, the transformation of L-Cys in cationic forms and their release to the electrolyte, as well as the accumulation of such metal ions in the sol-gel hybrid coating during exposure in NaCl, will decrease the corrosion resistance of the sol-gel hybrid system (GPTMS-TMOS precursor + 0.3% L-Cys + 0.6% ZrO<sub>2</sub>).

It could be concluded, after the revision of above results, reported in the literature, that there are several characteristics of ZrO<sub>2</sub> and L-Cyst, which should be taken into account before introducing as dopants in GPTMS-TMOS precursor, because their behavior is influenced by the pH changes of the solution at the interface of AZ61-sol-gel-electrolyte, including: Zeta potential (surface charge); chemisorption and

desorption processes; internal stress in the sol-gel precursor (GPTMS-TMOS), as well as the change in its structure, after the introduction of particles of ZrO<sub>2</sub> and L-cys and their encapsulation. Based on the results presented in our study, we cannot recommend their use as dopants in GPTMS-TMOS precursor.

#### 4. CONCLUSIONS

- Sol-gel coatings based on GPTMS-TMOS precursor, including as dopants L-Cysteine and ZrO<sub>2</sub> in different concentrations, were applied on the surface of AZ61 magnesium alloy. The corrosion resistance of the formed dip-coated hybrid systems was studied in 0.6M NaCl solution, by immersion for up 14 days. XRD spectra revealed that the main corrosion product on the coated surface was Mg(OH)<sub>2</sub> brucite, while on the untreated AZ61 surface, in addition to brucite, there were several compounds of Zn with chloride, in the presence of NaCl. The corrosion attack on the untreated AZ61 surface is well localised, expressed by cracks and caverns, while on the dip-coated surface the corrosion attack mostly occurs through pitting with a different diameter size.
- Two non-destructive electrochemical methods were employed, contrasting the electrochemical behaviour of the dip-coated AZ61 with that of uncoated alloy. The tendency in the changes of the corrosion potential at open circuit correlated positively with SEM-EDS and XRD analysis of the surface. The EIS diagrams provided additional information and the results obtained were fitted to an equivalent-circuit model. Based on the Bode diagram of EIS, the corrosion resistance  $R_{corr}$  ( $R_s + R_{ct}$ ) values were calculated.

They showed that after exposure for 14 days in 0.6M NaCl the values of  $R_{corr}$  significantly decreased.

- A possible explanation of the results reported in this study is that the behavior of ZrO<sub>2</sub> and L-Cysteine, used as dopants in GPTMS-TMOS precursor, is influenced by the pH changes of the solution at the interface of AZ61-sol-gel coating-electrolyte, including: Zeta potential (surface charge) of the dopants; chemisorption and desorption processes; internal stress in the sol-gel precursor, as well as the change in its structure, after introduction of particles of ZrO<sub>2</sub> and L-cys and their encapsulation.

## ACKNOWLEDGMENTS

L. Hernández gratefully thanks CONACYT for his scholarship as Ph.D. student at CINVESTAV-IPN and for the research stay at CENIM/CSIC (the National Center for metallurgical Research of Madrid, Spain). The authors acknowledge LANNBIO-CINVESTAV for permitting the use of their facilities, as well to D. Aguilar-Treviño, D. Huerta-Quintanilla, and G. Espinoza-Gurriz for their technical assistance.

## REFERENCES

- Afrin, N., Chen, D.L., Cao, X., Jahazi, M. (2008). Microstructure and tensile properties of friction stir welded AZ31B magnesium alloy. *Mat. Sci. Eng. A* 472 (1–2), 179–186. <https://doi.org/10.1016/j.msea.2007.03.018>.
- Aperador Chaparro, W., Rodríguez Zamora, G., Franco, F. (2012). Comportamiento de la corrosión de aleaciones de magnesio AZ31-B en ambiente marino, modificadas por el proceso de fricción-agitación. *Ingeniare. Rev. Chil. Ing.* 20 (1), 119–125. <https://doi.org/10.4067/S0718-33052012000100012>.
- Asmussen, R.M., Binns, W.J., Partovi-Nia, R., Jakupi, P., Shoosmith, D.W. (2016). The stability of aluminum-manganese intermetallic phases under the microgalvanic coupling conditions anticipated in magnesium alloys. *Mater. Corros.* 67 (1), 39–50. <https://doi.org/10.1002/maco.201508349>.
- Atik, M., Zarzycki, J. (1994). Protective TiO<sub>2</sub>-SiO<sub>2</sub> coatings on stainless steel sheets prepared by dip-coating. *J. Mater. Sci. Lett.* 13 (17), 1301–1304. <https://doi.org/10.1007/BF00270967>.
- Atik, M., De Lima Neto, P., Aegerter, M.A., Avaca, L.A. (1995). Sol-gel TiO<sub>2</sub>-SiO<sub>2</sub> films as protective coatings against corrosion of 316L stainless steel in H<sub>2</sub>SO<sub>4</sub> solutions. *J. Appl. Electrochem.* 25 (2), 142–148. <https://doi.org/10.1007/BF00248171>.
- Barranco, V., Carmona, N., Galván, J.C., Grobelny, M., Kwiatkowski, L., Villegas, M.A. (2010). Electrochemical study of tailored sol-gel thin films as pre-treatment prior to organic coating for AZ91 magnesium alloy. *Prog. Org. Coat.* 68 (4), 347–355. <https://doi.org/10.1016/j.porgcoat.2010.02.009>.
- Barranco, V., El hadad, A.A., Jiménez-Morales, A., Peón, E., Hickman, G.J., Perry, C.C., Galván, J.C. (2014a). Enhancing in vitro biocompatibility and corrosion protection of organic-inorganic hybrid sol-gel films with nanocrystalline hydroxyapatite. *J. Mater. Chem. B* 2 (24), 3886–3896. <https://doi.org/10.1039/C4TB00173G>.
- Barranco, V., Jiménez-Morales, A., Hickman, G. J., Galván, J. C., Perry, C. C., El hadad, A.A. (2014b). Triethylphosphite as a network forming agent enhances in vitro biocompatibility and corrosion protection of hybrid organic-inorganic sol-gel coatings for Ti6Al4V alloys. *J. Mater. Chem. B* 2 (45), 7955–7963. <https://doi.org/10.1039/C4TB01175A>.
- Behzadnasab, M., Mirabedini, S.M., Kabiri, K., Jamali, S. (2011). Corrosion performance of epoxy coatings containing silane treated ZrO<sub>2</sub> nanoparticles on mild steel in 3.5% NaCl solution. *Corros. Sci.* 53 (1), 89–98. <https://doi.org/10.1016/j.corsci.2010.09.026>.
- Caruso, R., Díaz-Parralejo, A., Miranda, P., Guiberteau, F. (2001). Controlled preparation and characterization of multilayer sol-gel zirconia dip-coatings. *J. Mater. Res.* 16 (8), 2391–2398. <https://doi.org/10.1557/JMR.2001.0328>.
- Chen, Y., Jin, L., Xie, Y. (1998). Sol-Gel processing of organic-inorganic nanocomposite protective coatings. *J. Sol-Gel Sci. Techn.* 13 (1–3), 735–738. <https://doi.org/10.1023/A:1008657408992>.
- Córdoba, L., Montemor, M., Coradin, T. (2016). Silane/TiO<sub>2</sub> coating to control the corrosion rate of magnesium alloys in simulated body fluid. *Corros. Sci.* 104, 152–161. <https://doi.org/10.1016/j.corsci.2015.12.006>.
- De Lima Neto, P., Atik, M., Avaca, L.A., Aegerter, M.A. (1994). Sol-gel coatings for chemical protection of stainless steel. *J. Sol-gel Sci. Techn.* 2 (1–3), 529–534. <https://doi.org/10.1007/BF00486303>.
- El-Hadad, A.A., Barranco, V., Samaniego, A., Llorente, I., García-Galván, F.R., Jiménez-Morales, A., Galván, J.C., Feliu Jr., S. (2014). Influence of substrate composition on corrosion protection of sol-gel thin films on magnesium alloys in 0.6 M NaCl aqueous solution. *Prog. Org. Coat.* 7 (11), 1642–1652. <https://doi.org/10.1016/j.porgcoat.2014.05.026>.
- Gallardo, J., Duran, A., Garcia, I., Celis, J.P., Arenas, M.A., Conde, A. (2003). Effect of sintering temperature on the corrosion and wear behavior of protective SiO<sub>2</sub>-based sol-gel coatings. *J. Sol-Gel Sci. Techn.* 27 (2), 175–183. <https://doi.org/10.1023/A:1023702701850>.
- García-Heras, M., Jiménez-Morales, A., Casal, B., Galván, J.C., Radzki, S., Villegas, M.A. (2004). Preparation and electrochemical study of cerium-silica sol-gel thin films. *J. Alloys Compd.* 380 (1–2), 219–224. <https://doi.org/10.1016/j.jallcom.2004.03.047>.
- Gomez-Romero, P. (2001). Hybrid organic-inorganic materials—in search of synergic activity. *Adv. Mater.* 13 (3), 163–174. [https://doi.org/10.1002/1521-4095\(200102\)13:3<163::AID-ADMA163>3.0.CO;2-U](https://doi.org/10.1002/1521-4095(200102)13:3<163::AID-ADMA163>3.0.CO;2-U).
- Gray, J., Luan, B. (2002). Protective coatings on magnesium and its alloys—a critical review. *J. Alloys Compd.* 336 (1–2), 88–113. [https://doi.org/10.1016/S0925-8388\(01\)01899-0](https://doi.org/10.1016/S0925-8388(01)01899-0).
- Guo, X., An, M., Yang, P., Li, H., Su, C. (2009). Effects of benzotriazole on anodized film formed on AZ31B magnesium alloy in environmental-friendly electrolyte. *J. Alloys Compd.* 482 (1–2), 487–497. <https://doi.org/10.1016/j.jallcom.2009.04.053>.
- Gusmano, G., Montesperelli, G., Rapone, M., Padeletti, G., Cusmà, A., Kaciulis, S., Mezzi, A., Di Maggio, R. (2007). Zirconia primers for corrosion resistant coatings. *Surf. Coat. Tech.* 201 (12), 5822–5828. <https://doi.org/10.1016/j.surfcoat.2006.10.036>.
- Hamu, G.B., Eliezer, D., Wagner, L. (2009). The relation between severe plastic deformation microstructure and corrosion behavior of AZ31 magnesium alloy. *J. Alloys Compd.* 468 (1–2), 222–229. <https://doi.org/10.1016/j.jallcom.2008.01.084>.
- Han, G., Liu, X. (2016). Phase control and formation mechanism of Al-Mn(-Fe) intermetallic particles in Mg-Al-based alloys with FeCl<sub>3</sub> addition or melt superheating. *Acta Mater.* 114, 54–66. <https://doi.org/10.1016/j.actamat.2016.05.012>.
- Hernández-Alvarado, L.A., Lomelí, M.A., Hernández, L.S., Miranda, J.M., Narváez, L., Díaz, I., García-Alonso, M.C., Escudero, M.L. (2014). Caracterización y comportamiento frente a la corrosión de recubrimientos de ácido fítico, obtenidos por conversión química, sobre substratos de magnesio en solución fisiológica. *Rev. Metal.* 50 (2), e012. <https://doi.org/10.3989/revmetalm.012>.

- ISO 8407 (1991). Corrosion of metals and alloys -- Removal of corrosion products from corrosion test specimens. International Organization for Standardization, Genève.
- Jiménez-Morales, A., Galván, J.C., Aranda, P. (2002). A new silver-ion selective sensor based on a polythiacrown-ether entrapped by sol-gel. *Electrochim. Acta* 47 (13–14), 2281–2287. [https://doi.org/10.1016/S0013-4686\(02\)00068-3](https://doi.org/10.1016/S0013-4686(02)00068-3).
- Judeinstein, P., Sanchez, C. (1996). Hybrid organic-inorganic materials: a land of multidisciplinary. *J. Mater. Chem.* 6 (4), 511–525. <https://doi.org/10.1039/JM9960600511>.
- Kahraman, M.V., Kugu, M., Menciloğlu, Y., Kayaman-Apohan, N., Güngör, A. (2006). The novel use of organoalkoxy silane for the synthesis of organic-inorganic hybrid coatings. *J. Non-Cryst. Solids* 352 (21–22), 2143–2151. <https://doi.org/10.1016/j.jnoncrsol.2006.02.029>.
- Liu, H., Sun, X., Yin, C., Hu, C. (2008). Removal of phosphate by mesoporous ZrO<sub>2</sub>. *J. Hazard. Mater.* 151 (2–3), 616–622. <https://doi.org/10.1016/j.jhazmat.2007.06.033>.
- Liu, X., Huang, Y., Yang, J. (2002). Effect of rheological properties of the suspension on the mechanical strength of Al<sub>2</sub>O<sub>3</sub>-ZrO<sub>2</sub> composites prepared by gelcasting. *Ceram. Int.* 28 (2), 159–164. [https://doi.org/10.1016/S0272-8842\(01\)00072-4](https://doi.org/10.1016/S0272-8842(01)00072-4).
- Liu, X., Yue, Z., Romeo, T., Weber, J., Scheuermann, T., Moulton, S., Wallace, G. (2013). Biofunctionalized anti-corrosive silane coatings for magnesium alloys. *Acta Biomater.* 9 (10), 8671–8677. <https://doi.org/10.1016/j.actbio.2012.12.025>.
- Luo, J., Cui, N. (1998). Effects of microencapsulation on the electrode behavior of Mg<sub>2</sub>Ni-based hydrogen storage alloy in alkaline solution. *J. Alloys Compd.* 264 (1–2), 299–305. [https://doi.org/10.1016/S0925-8388\(97\)00277-6](https://doi.org/10.1016/S0925-8388(97)00277-6).
- Ma, X., Guo, Q., Xie, Y., Ma, H. (2016). Green chemistry for the preparation of L-cysteine functionalized silver nanoflowers. *Chem. Phys. Lett.* 652, 148–151. <https://doi.org/10.1016/j.cplett.2016.04.004>.
- Minti, H., Eyal, M., Reisfeld, R., Berkovic, G. (1991). Quantum dots of cadmium sulfide in thin glass films prepared by sol-gel technique. *Chem. Phys. Lett.* 183 (3–4), 277–282. [https://doi.org/10.1016/0009-2614\(91\)80063-4](https://doi.org/10.1016/0009-2614(91)80063-4).
- Mirabedini, S., Behzadnasab, M., Kabiri, K. (2012). Effect of various combinations of zirconia and organoclay nanoparticles on mechanical and thermal properties of an epoxy nanocomposite coating. *Compos. Part A Appl. Sci. Manuf.* 43 (11), 2095–2106. <https://doi.org/10.1016/j.compositesa.2012.07.002>.
- Mocanu, A., Cernica, I., Tomoaia, G., Bobos, L. D., Horovitz, O., Tomoaia-Cotisel, M. (2009). Self-assembly characteristics of gold nanoparticles in the presence of cysteine. *Colloid Surface A* 338 (1–3), 93–101. <https://doi.org/10.1016/j.colsurfa.2008.12.041>.
- Montoya, P., Martins, C.R., de melo, H.G., Aoki, I.V., Jaramillo, F., Calderón, J.A. (2014). Synthesis of polypyrrole-magnesium/silane coatings on steel and assessment of anticorrosive properties. *Electrochim. Acta* 124, 100–108. <https://doi.org/10.1016/j.electacta.2013.07.105>.
- Novak, B.M. (1993). Hybrid nanocomposite materials—between inorganic glasses and organic polymers. *Adv. Mater.* 5 (6), 422–433. <https://doi.org/10.1002/adma.19930050603>.
- Pan, F., Feng, Z., Zhang, X., Tang, A. (2012). The types and distribution characterization of Al-Mn phases in the AZ61 magnesium alloy. *Procedia Engineer.* 27, 833–839. <https://doi.org/10.1016/j.proeng.2011.12.528>.
- Park, M., Lee, J. E., Park, C. G., Ho Lee, S., Kwang Seok, H., Bin Choy, Y. (2013). Polycaprolactone coating with varying thicknesses for controlled corrosion of magnesium. *J. Coat. Technol. Res.* 10 (5), 695–706. <https://doi.org/10.1007/s11998-013-9474-6>.
- Radhakrishnan, S., Siju, C.R., Mahanta, D., Patil, S., Madras, G. (2009). Conducting polyaniline-nano-TiO<sub>2</sub> composites for smart corrosion resistant coatings. *Electrochim. Acta* 54 (4), 1249–1254. <https://doi.org/10.1016/j.electacta.2008.08.069>.
- Rueda, L.M., Hernández, C.A., Viejo, F., Coy, A.E., Mosa, J., Aparicio, M. (2016). Diseño de recubrimientos multicapa barrera-biomimético base TEOS-GPTMS sobre la aleación de magnesio Elektron 21 de potencial aplicación en la fabricación de implantes ortopédicos. *Rev. Metal.* 52 (3), e075. <https://doi.org/10.3989/revmetalm.075>.
- Sayilkan, H., Şener, Ş., Şener, E., Sülü, M. (2003). The sol-gel synthesis and application of some anticorrosive coating materials. *Mater. Sci.* 39 (5), 733–739. <https://doi.org/10.1023/B:MASC.0000023514.74970.73>.
- Shchukin, D.G., Zheludkevich, M., Yasakau, K., Lamaka, S., Ferreira, M.G.S., Möhwald, H. (2006). Layer-by-layer assembled nanocontainers for self-healing corrosion protection. *Adv. Mater.* 18 (13), 1672–1678. <https://doi.org/10.1002/adma.200502053>.
- Stein, A., Melde, B.J., Schroden, R.C. (2000). Hybrid inorganic-organic mesoporous silicates—nanoscopic reactors coming of age. *Adv. Mater.* 12 (19), 1403–1419. [https://doi.org/10.1002/1521-4095\(200010\)12:19<1403::AID-ADMA1403>3.0.CO;2-X](https://doi.org/10.1002/1521-4095(200010)12:19<1403::AID-ADMA1403>3.0.CO;2-X).
- Storey, R.F., Rawlins, J.W. (2014). *The Waterborne Symposium. In Proceedings of the forty-first annual international waterborne, highsolids, and powder coating symposium.* Lulu Press Inc, New Orleans, LA, February.
- Sunwoo, S., Kim, J.H., Lee, K.G., Kim, H. (2000). Preparation of ZrO<sub>2</sub> coated graphite powders. *J. Mater. Sci.* 35 (14), 3677–3680. <https://doi.org/10.1023/A:1004894404376>.
- Supplit, R., Koch, T., Schubert, U. (2007). Evaluation of the anti-corrosive effect of acid pickling and sol-gel coating on magnesium AZ31 alloy. *Corros. Sci.* 49 (7), 3015–3023. <https://doi.org/10.1016/j.corsci.2007.02.006>.
- Tamar, Y., Mandler, D. (2008). Corrosion inhibition of magnesium by combined zirconia silica sol-gel films. *Electrochim. Acta* 53 (16), 5118–5127. <https://doi.org/10.1016/j.electacta.2008.02.029>.
- Tan, A., Soutar, A.M., Annergren, I.F., Liu, Y.N. (2005). Multilayer sol-gel coatings for corrosion protection of magnesium. *Surf. Coat. Tech.* 198 (1–3), 478–482. <https://doi.org/10.1016/j.surfcoat.2004.10.066>.
- Wang, D., Bierwagen, G.P. (2009). Sol-gel coatings on metals for corrosion protection. *Prog. Org. Coat.* 64 (4), 327–338. <https://doi.org/10.1016/j.porgcoat.2008.08.010>.
- Wang, H., Shi, Z. (2011). In vitro biodegradation behavior of magnesium and magnesium alloy. *J. Biomed. Mater. Res.* 98B (2), 203–209. <https://doi.org/10.1002/jbm.b.31769>.
- Zhang, X., Wang, F., Du, Y. (2007). Effect of nano-sized titanium powder addition on corrosion performance of epoxy coatings. *Surf. Coat. Tech.* 201 (16–17), 7241–7245. <https://doi.org/10.1016/j.surfcoat.2007.01.042>.
- Zhang, S., Zhang, X., Zhao, C., Li, J., Song, Y., Xie, C., Tao, H., Zhang, Y., He, Y., Jiang, Y., Bian, Y. (2010). Research on an Mg-Zn alloy as a degradable biomaterial. *Acta Biomater.* 6 (2), 626–640. <https://doi.org/10.1016/j.actbio.2009.06.028>.
- Zhang, L., Xu, C., Song, G., Li, B. (2015). Self-assembly of L-cysteine-gold nanoparticles as chiral probes for visual recognition of 3, 4-dihydroxyphenylalanine enantiomers. *RSC Adv.* 5 (34), 27003–27008. <https://doi.org/10.1039/C5RA01271F>.
- Zheludkevich, M., Miranda Salvado, I., Ferreira, M.G.S. (2005). Sol-gel coatings for corrosion protection of metals. *J. Mater. Chem.* 15 (48), 5099–5111. <https://doi.org/10.1039/B419153F>.
- Zheludkevich, M.L., Serra, R., Montemor, M.F., Miranda Salvado, I.M., Ferreira, M.G.S. (2006). Corrosion protective properties of nanostructured sol-gel hybrid coatings to AA2024-T3. *Surf. Coat. Tech.* 200 (9), 3084–3094. <https://doi.org/10.1016/j.surfcoat.2004.09.007>.
- Zhong, X., Li, Q., Hu, J., Lu, Y. (2008). Characterization and corrosion studies of ceria thin film based on fluorinated AZ91D magnesium alloy. *Corros. Sci.* 50 (8), 2304–2309. <https://doi.org/10.1016/j.corsci.2008.05.016>.